Analytical Model and Fault Analysis in 3×3 Phase Permanent Magnet Synchronous Machine

Author: Aeishwarya Baviskar
Technical University of Munich

Supervisor: Dipl.-Ing Jörge Kammermann
Technical University of Munich

***Abstract*—Multiphase machines, especially N×3 phase machines showcase a better fault tolerance as compared to 3 phase machines and also have a higher reliability. In addition to their use in high power applications such as hybrid/electric vehicles, ship propulsion etc. have drawn serious interest towards the study of these machines. This paper attempts to present a dq equivalent model of a 3×3 Permanent magnet synchronous machine (PMSM) which can be further used to develop control techniques for 3×3 phase PMSM. A frequency domain analysis of mutual coupling between different phases is also presented. In addition, the machine model is simulated in Matlab Simulink and three kinds of faults, namely switching failure, open phase fault and phase-to-phase short circuit fault are studied. It also attempts to analyze the machine in post fault conditions.**

***Index Terms*—3×3 phase PMSM, dq model, switching failure, open phase fault, phase-to-phase short circuit**

I. Introduction

Multiphase machines were conceptualized in the 1920s heeding to the demand for high power generators. The primary objective was to overcome the constraint on allowable current capacity in circuit breakers. Since then, multiphase machines have been under scrutiny and have gradually developed due to their inherent advantages over 3-phase machines. One of the main advantages was the high frequency torque ripple in variable frequency drives. But the development of pulse width modulation techniques have rendered it less significant. Other attractive features for the increased attention towards development of multiphase machines include reduction in stator current per phase, reduced harmonic currents, reduced per phase power rating and higher efficiency [1]–[4]. Multiphase machines are predominantly used in high power applications such as ship propulsion, electric aircraft, hybrid vehicles, turbo compressors and ultra high speed elevators [5].

The subtle difference between a multiphase winding and a N×3-phase winding is shown in *Figure* 1. For a multiphase winding all the phases are electrically connected in a star connection. A N×3 phase windings, on the other hand, are electrically isolated phase windings (generally 3 phase) which have a magnetic coupling between them [4]. Thus, a N×3 phase machine can be operated, at a lesser power, even when one of the N-phases is disconnected. This gives a distinct advantage for operation in fault scenario and increases the reliability of the machine. Authors in [6] provide a further analysis of N×3 phase winding machines.

The most common modeling approaches for multiphase winding machines are vector space decomposition [7] and the dq frame model [2], [4]–[6], [8], [9]. Finite element analysis is also an approach but it requires higher computation effort. The dq reference frame model paves way towards easy implementation of control on the machine [5], hence, it is used in this work.

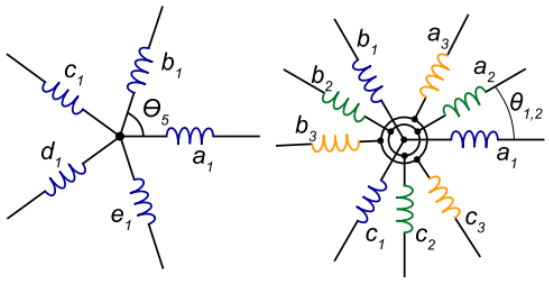

Fig. 1. 5 Phase winding and 3×3 phase winding [4]

Statistical studies conducted on industrial motors (mainly induction machines) conclude that bearing fault is one of the most common type of fault in machines, the next in order being stator faults (stator winding fault) [10]. Studies also reveal that machine is less likely to bear a rotor or a mechanical fault [11]. Although most of the studies are conducted on induction machines, considering the similarities in the construction of induction machines and permanent magnet synchronous machines, parallels can be drawn between them. Authors in [12] argue that power electronics is the most vulnerable part in a drive system. They have investigated the fault modes of a voltage fed inverter in induction motor drive. Finite element analysis is also used to study faults in PMSMs [13], [14]. Finite element analysis becomes necessary when simulating rotor faults such as eccentricity, demagnetization or a broken magnet. Faults such as the short-circuit or open-circuit can be satisfactorily analyzed through analytical models as presented in [2], [4].

Although a lot of different kinds of fault detection methods have been presented in [10], [15]–[19], it is imperative to recognize the fault signatures in the current or torque for most methods [20], [21]. Hence, this work attempts to develop a dq reference model of the 3×3 phase permanent magnet synchronous machine with field oriented control, simulate three faults and analyze their current signatures through a harmonic analysis. It should be noted that fault detection through harmonics is not only limited to stator and or short

circuit and open-circuit faults [19]. The three faults considered in this work are open phase fault, phase-to-phase short circuit fault and switching failure in the power electronic.

This paper is divided into 5 sections. Section I is the introduction, Section II provides the dq model of the 3×3 phase PMSM. Section II-B is dedicated to the analysis of mutual couplings between the windings. A few details regarding the simulation of the proposed model in Simulink are given in Section III. Section IV presents the result of the fault simulations and its analysis. The final section (Section V) attempts to draw a few conclusions from the observations during this work.

II. Analytical Model of a 3×3 Phase PMSM

Consider *Figure* 2 which shows the 3×3 phase windings in the machine. $a_1b_1c_1$ is the first 3 phase winding, $a_2b_2c_2$ the second and $a_3b_3c_3$ the third three phase winding. They are separated by a mechanical angle of $\theta = 30$ degrees. θ_r is the angle between the a_1 axis and the q axis. It is assumed that the winding distribution is sinusoidal. The eddy current, hysteresis, and core losses are neglected and only the fundamental component of the air gap flux is considered for the analysis. The dq frame reference model for a PMSM can

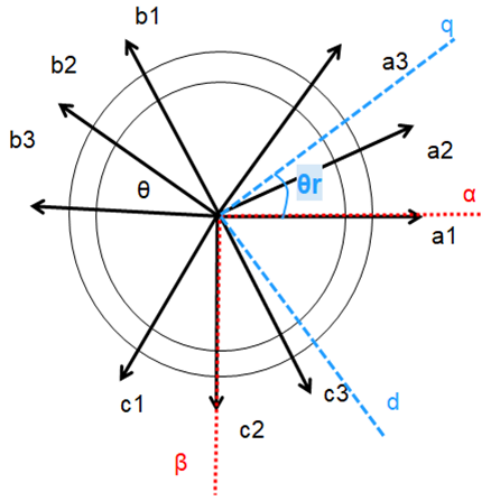

Fig. 2. Phase winding for a 3×3 phase machine indicating $\alpha\beta$ and dq axis

be written as follows,

$$v_{d1} = r_s i_{d1} + \frac{d\psi_{d1}}{dt} - \omega\psi_{q1} \tag{1}$$

$$v_{q1} = r_s i_{q1} + \frac{d\psi_{q1}}{dt} + \omega\psi_{d1} \tag{2}$$

with only one coil, the flux linkages ψ_{d1} and ψ_{q1} can be given as follows,

$$\psi_{d1} = \Psi_{Md1} + L_{d1} i_{d1} \tag{3}$$

$$\psi_{q1} = L_{q1} i_{q1} \tag{4}$$

with 3 coils, the flux linkages represent all the mutual couplings between the windings and can be written as,

$$\psi_{d1} = \Psi_{Md1} + L_{d1} i_{d1} + M_{d1d2} i_{d2} + M_{d1d3} i_{d3} \tag{5}$$

$$\psi_{q1} = L_{q1} i_{q1} + M_{q1q2} i_{q2} + M_{q1q3} i_{q3} \tag{6}$$

According to [6] the mechanical angle separation ($\theta = 30$ in this case) influences the mutual inductance between the different winding phases. For a balanced operation of the machine it is necessary that the d axis and q axis components of individual winding phases be equal. Thus, [6] discards some of the angles for construction of the 3×3 phase machine. However, with the values of leakage and mutual inductance considered in this work, which is adapted from [2], the imbalance in the dq axis components is insignificant and $\theta = 30$ can be assumed. The Equations in phase domain are as follows,

$$\underline{V}_1 = r_s \underline{i}_1 + L_1 \frac{d\underline{i}_1}{dt} + L_2 \frac{d\underline{i}_2}{dt} + L_3 \frac{d\underline{i}_3}{dt} + \begin{bmatrix} cos(\omega_e t) \\ cos(\omega_e t - \frac{2\pi}{3}) \\ cos(\omega_e t - \frac{4\pi}{3})) \end{bmatrix} \lambda_{pm}\omega_e \tag{7}$$

$$\underline{V}_2 = r_s \underline{i}_2 + L_1 \frac{d\underline{i}_2}{dt} + L_2^T \frac{d\underline{i}_1}{dt} + L_2 \frac{d\underline{i}_3}{dt} + \begin{bmatrix} cos(\omega_e t - \frac{\pi}{6}) \\ cos(\omega_e t - \frac{5\pi}{6}) \\ cos(\omega_e t - \frac{5\pi}{3}) \end{bmatrix} \lambda_{pm}\omega_e \tag{8}$$

$$\underline{V}_3 = r_s \underline{i}_3 + L_1 \frac{d\underline{i}_3}{dt} + L_2^T \frac{d\underline{i}_1}{dt} + L_3^T \frac{d\underline{i}_2}{dt} + \begin{bmatrix} cos(\omega_e t - \frac{\pi}{3}) \\ cos(\omega_e t - \pi) \\ cos(\omega_e t - \frac{11\pi}{6})) \end{bmatrix} \lambda_{pm}\omega_e \tag{9}$$

where,

$$\underline{V}_k = \begin{bmatrix} V_{ak} \\ V_{bk} \\ V_{ck} \end{bmatrix}, \underline{i}_k = \begin{bmatrix} i_{ak} \\ i_{bk} \\ i_{ck} \end{bmatrix} \forall k = 1, 2, 3 \tag{10}$$

$$L_1 = \begin{bmatrix} L_l + \frac{3}{2}L_{ms} & 0 & 0 \\ 0 & L_l + \frac{3}{2}L_{ms} & 0 \\ 0 & 0 & L_l + \frac{3}{2}L_{ms} \end{bmatrix} \tag{11}$$

$$L_2 = \begin{bmatrix} -L_{lm} - \frac{\sqrt{3}}{2}L_{ms} & L_{lm} + \frac{\sqrt{3}}{2}L_{ms} & 0 \\ 0 & -L_{lm} - \frac{\sqrt{3}}{2}L_{ms} & L_{lm} + \frac{\sqrt{3}}{2}L_{ms} \\ L_{lm} + \frac{\sqrt{3}}{2}L_{ms} & 0 & -L_{lm} - \frac{\sqrt{3}}{2}L_{ms} \end{bmatrix} \tag{12}$$

$$L_3 = \begin{bmatrix} 0 & \frac{1}{2}L_{ms} & 0 \\ 0 & 0 & \frac{1}{2}L_{ms} \\ \frac{1}{2}L_{ms} & 0 & 0 \end{bmatrix} \tag{13}$$

r_s is the winding resistance, L_{ms} is the mutual inductance, L_{lm} is the mutual inductance between two winding sets, and L_l is the leakage inductance. λ_{pm} is the field strength of the permanent magnet and ω_e is the synchronous frequency. To convert (7), (8), and (9) to synchronous reference frame (dq), they must be converted first to the stationary reference frame ($\alpha\beta$). The following matrices are used to convert the kth phase winding to stationary reference frame respectively.

$$T_1 = \frac{2}{3}\begin{bmatrix} 1 & -\frac{1}{2} & -\frac{1}{2} \\ 0 & -\frac{\sqrt{3}}{2} & \frac{\sqrt{3}}{2} \\ \frac{1}{2} & \frac{1}{2} & \frac{1}{2} \end{bmatrix}, T_2 = \frac{2}{3}\begin{bmatrix} \frac{\sqrt{3}}{2} & -\frac{\sqrt{3}}{2} & 0 \\ -\frac{1}{2} & -\frac{1}{2} & 1 \\ \frac{1}{2} & \frac{1}{2} & \frac{1}{2} \end{bmatrix}$$

$$T_3 = \frac{2}{3}\begin{bmatrix} \frac{1}{2} & -1 & \frac{1}{2} \\ -\frac{\sqrt{3}}{2} & 0 & \frac{\sqrt{3}}{2} \\ \frac{1}{2} & \frac{1}{2} & \frac{1}{2} \end{bmatrix}$$

$$V_{\alpha\beta_k} = T_k V_k, \forall k = 1, 2, 3 \tag{14}$$

where $V_{\alpha\beta_k}$ is the voltage in the stationary reference frame ($\alpha\beta$ axis in *Figure* 2). The final step is to convert the $\alpha\beta$ frame of reference to the dq frame of reference using the following matrix.

$$T_{qq} = \begin{bmatrix} cos\theta_r & -sin\theta_r \\ sin\theta_r & cos\theta_r \end{bmatrix}$$

It is possible to write the voltage equations in dq frame of reference as,

$$\begin{aligned} \underline{V}_{dq1}(t) &= r_s \underline{i}_{dq1}(t) + L_0 \frac{d\underline{i}_{dq1}(t)}{dt} + L_0^T \begin{bmatrix} i_{d1}\omega_e \\ -i_{q1}\omega_e \end{bmatrix} \\ &+ L_1 \frac{d\underline{i}_{dq2}(t)}{dt} + L_1^T \begin{bmatrix} i_{d2}\omega_e \\ -i_{q2}\omega_e \end{bmatrix} + L_2 \frac{d\underline{i}_{dq3}(t)}{dt} \\ &+ L_2^T \begin{bmatrix} i_{d3}\omega_e \\ -i_{q3}\omega_e \end{bmatrix} + \lambda_{pm}\omega_e \begin{bmatrix} 1 \\ 0 \end{bmatrix} \end{aligned} \tag{15}$$

$$\begin{aligned} \underline{V}_{dq2}(t) &= r_s \underline{i}_{dq2}(t) + L_0 \frac{d\underline{i}_{dq2}(t)}{dt} + L_0^T \begin{bmatrix} i_{d2}\omega_e \\ -i_{q2}\omega_e \end{bmatrix} \\ &+ L_1 \frac{d\underline{i}_{dq2}(t)}{dt} + L_1^T \begin{bmatrix} i_{d2}\omega_e \\ -i_{q2}\omega_e \end{bmatrix} + L_1 \frac{d\underline{i}_{dq3}(t)}{dt} \\ &+ L_1^T \begin{bmatrix} i_{d3}\omega_e \\ -i_{q3}\omega_e \end{bmatrix} + \lambda_{pm}\omega_e \begin{bmatrix} 1 \\ 0 \end{bmatrix} \end{aligned} \tag{16}$$

$$\begin{aligned} \underline{V}_{dq3}(t) &= r_s \underline{i}_{dq3}(t) + L_0 \frac{d\underline{i}_{dq3}(t)}{dt} + L_0^T \begin{bmatrix} i_{d3}\omega_e \\ -i_{q3}\omega_e \end{bmatrix} \\ &+ L_2 \frac{d\underline{i}_{dq1}(t)}{dt} + L_2^T \begin{bmatrix} i_{d1}\omega_e \\ -i_{q1}\omega_e \end{bmatrix} + L_1 \frac{d\underline{i}_{dq2}(t)}{dt} \\ &+ L_1^T \begin{bmatrix} i_{d2}\omega_e \\ -i_{q2}\omega_e \end{bmatrix} + \lambda_{pm}\omega_e \begin{bmatrix} 1 \\ 0 \end{bmatrix} \end{aligned} \tag{17}$$

where,

$$\underline{V}_{dq_k} = \begin{bmatrix} V_{dk} \\ V_{qk} \end{bmatrix}, \underline{i}_{dq_k} = \begin{bmatrix} i_{dk} \\ i_{qk} \end{bmatrix}, \forall k = 1, 2, 3 \tag{18}$$

$$L_0 = \begin{bmatrix} L_l + \frac{3}{2}L_{ms} & 0 \\ 0 & L_l + \frac{3}{2}L_{ms} \end{bmatrix} \tag{19}$$

$$L_1 = \begin{bmatrix} \sqrt{3}L_{lm} + \frac{3}{2}L_{ms} & 0 \\ 0 & \sqrt{3}L_{lm} + \frac{3}{2}L_{ms} \end{bmatrix} \tag{20}$$

$$L_2 = \begin{bmatrix} 2L_{lm} + \frac{3}{2}L_{ms} & 0 \\ 0 & 2L_{lm} + \frac{3}{2}L_{ms} \end{bmatrix} \tag{21}$$

The torque equation is thus given by, (assuming $L_1 \approx L_2$ for a round rotor machine)

$$T_e = \frac{3}{2}\frac{P}{2}\lambda_{pm}(i_{q1} + i_{q2} + i_{q3}) \tag{22}$$

where, T_e is the electrical torque produced and P is the no of pole pairs.

$$T_e = J\frac{d\omega_e}{dt} + B\omega_e + T_m \tag{23}$$

where, T_m is the mechanical torque required for a motor and torque applied for generator operation, J is the moment of inertia of the machine, ω_e is the synchronous frequency, and B is the frictional constant which is assumed zero in ideal case. Equation (23) represents the mechanical model of machine including the swing equation. From (23) the rotor speed and thus the angular position as given by (24) can be calculated.

$$\frac{d\theta_r}{dt} = \omega_e \tag{24}$$

A. Parameter Calculation

Authors in [2] have presented a method to calculate the parameters of an 2×3 phase PMSM using the parameters of a 3 phase PMSM. The method assumes that the number of turns in N×3 machine (2×3 in case of [2] and 3×3 in this work) are equal to a 3 phase machine in an and the values of the inductances are multiplied by appropriate constants to produce the parameters of desired multiphase machine. Thus, the parameters adapted from [2] used in this work are as follows,

$$L_l = 344.5\mu H, L_{lm} = 38\mu H, \tag{25}$$

$$L_{ms} = 641\mu H, r_s = 1.98\Omega \tag{26}$$

B. Frequency domain analysis of mutual couplings between phases

Rewriting (15), (16), and (17) with $\frac{\underline{i}_{dq_k}}{dt}$ on the left hand side we get the differential equation for the 3×3 phase machine. The differential equation for $\frac{\underline{i}_{dq_1}}{dt}$ can be written as follows,

$$\begin{aligned} \frac{d\underline{i}_{dq1}(t)}{dt} &= L_0^{-1}(\underline{V}_{dq1}(t) - r_s \underline{i}_{dq1}(t) - + L_0^T \begin{bmatrix} i_{d1}\omega_e \\ -i_{q1}\omega_e \end{bmatrix} \\ &- L_1 \frac{d\underline{i}_{dq2}(t)}{dt} - L_1^T \begin{bmatrix} i_{d2}\omega_e \\ -i_{q2}\omega_e \end{bmatrix} - L_2 \frac{d\underline{i}_{dq3}(t)}{dt} \\ &- L_2^T \begin{bmatrix} i_{d3}\omega_e \\ -i_{q3}\omega_e \end{bmatrix} - \lambda_{pm}\omega_e \begin{bmatrix} 1 \\ 0 \end{bmatrix}) \end{aligned} \tag{27}$$

Taking laplace transform of (27) we can get the transfer function of $\underline{I}_{dq_1}(s)$. Similarly solving for $\underline{I}_{dq_2}(s)$ and $\underline{I}_{dq_3}(s)$ we get all the current transfer functions. Since, the system represented by these transfer functions is MIMO it is difficult to use the classical control techniques such as root locus and bode plot and complex vector notations must be used to solve

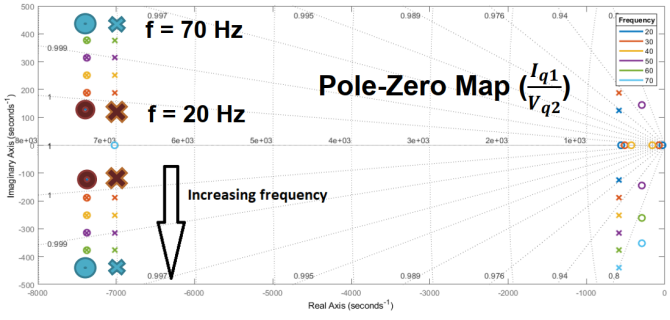

Fig. 3. Pole zero plot for I_{q1}/V_{q2} at different frequencies

these equations [2]. Although we can represent the transfer functions as,

$$I_{q_1} = G_1(s)V_{q_1} + G_2(s)V_{q_2} + G_3(s)V_{q_3} \quad (28)$$
$$+G_4(s)V_{d_1} + G_5(s)V_{d_2} + G_6(s)V_{d_3} \quad (29)$$

where $G_k(s)$ is a rational function in the frequency domain relating $\frac{I_{q_1}}{V_{q_k}}, \forall k = 1, 2, 3$ assuming the other two inputs to the system are zero. $G_2(s)$ is used to plot a pole zero map between $\frac{I_{q_1}}{V_{q_2}}$ as shown in *Figure* 3 with increasing synchronous frequency.

It is observed from the pole zero plot of I_{q_1}/V_{q_2} with

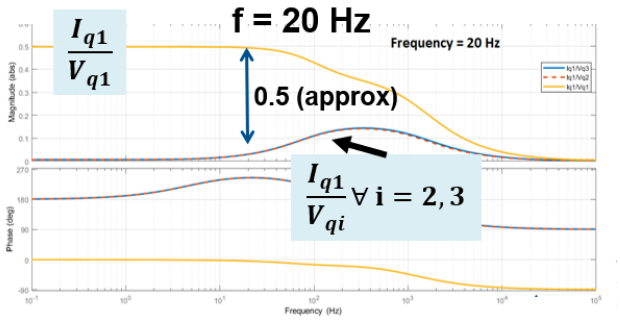

Fig. 4. Bode plot at $f_e = 20\ Hz$

increasing value of the synchronous frequency that the poles and zeros tend to go away from the imaginary axis as the frequency increases. Hence it can be implied using basic control theory that the damping in of transfer function $G_2(s)$ reduces with increasing frequency. Thus, at higher frequency the input V_{q_2} will have a higher influence on the quadrature axis current in phase 1 (i_{q1}), i.e. higher value of mutual couplings.

Figure 4 and 5 show the bode plots for $I_{q_1}/V_{q_k}, \forall k = 1, 2, 3$.

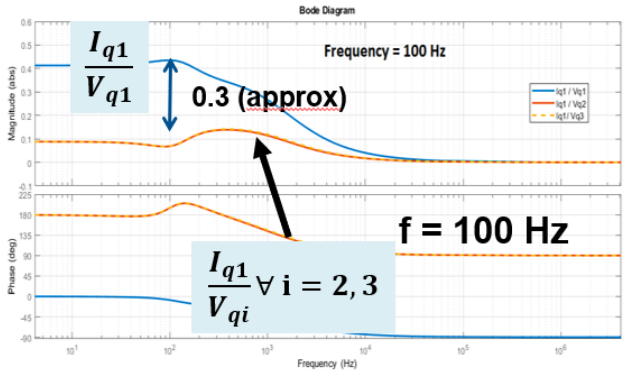

Fig. 5. Bode plot at $f_e = 100Hz$

It is observed from the bode plots that the magnitude of $I_{q_1}/V_{q_k}, \forall k = 2, 3$ is higher at $f_e = 100\ Hz$ as compared to $f_e = 20\ Hz$. Thus the bode plots reaffirm the conclusions drawn from the root locus diagram.

III. Simulink Model

Figure 6 shows the Simulink block for the simulation of (15), (16) and (17). It is followed by integrator blocks to calculate the currents in dq frame of reference. The voltage input in *Figure* 6 is as follows,

$$\underline{V}_{dq} = \begin{bmatrix} \underline{V}_{dq_1} \\ \underline{V}_{dq_2} \\ \underline{V}_{dq_3} \end{bmatrix}$$

The voltage is generated using a three phase inverter with

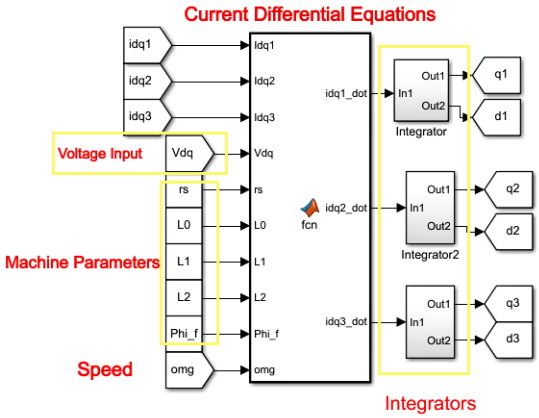

Fig. 6. Simulation of current differential equation

PWM switching. Field oriented control (FOC) is applied to the PMSM in order to obtain the desired torque and speed output. The main concept behind FOC is to assume the current in direct axis to be zero and calculate a reference quadrature axis current from the given inputs. This reference quadrature axis current is then used to produce a switching sequence (PWM in this case) for the inverter [22]. The reference or input mechanical torque given in this simulation is $1Nm$

Figure 7 shows the implementation of Equations (22), (23)

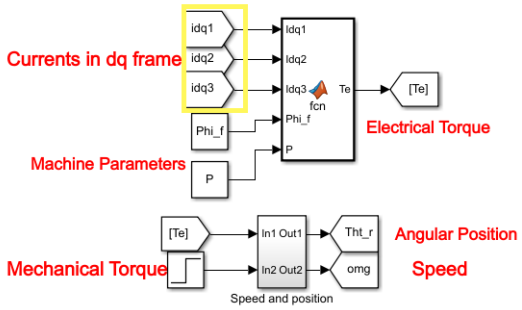

Fig. 7. Calculation of T_e, ω_e and θ_r

and (24).

IV. Fault Simulations and Analysis

As proposed in Section I three faults are being simulated on the 3×3 phase PMSM. Simulation of faults which require a finite element analysis are naturally eliminated due to the

choice of the modeling technique. The faults selected for simulation represent some of the most commonly occurring faults and/or the ones which can be simulated with sufficient accuracy given ideal conditions. It is to be noted that the phenomena such as failure of switches due to over current, current limitations on the switches, overheating of the machine in fault conditions and its effects on the functioning etc. are ignored. It is assume sufficiently large current capacity and heat tolerance in the wire as well.

A. *Switching Failure*

Switching failure is one of the most common types of faults in power electronics. It can occur due to failure of control circuit or can represent a fault in a particular switch which disables it to respond to the control input. *Figure* 8 shows the voltage waveform with a switching failure simulated at t = 0.7 sec. The state of the machine before the failure is assumed to be steady state. As shown in *Figure* 8, one of the switches from a voltage leg (V_{a1}) of the inverter fails to turn on and hence, there is only a negative voltage output at V_{a1}. It can be inferred from this voltage waveform that the current in the corresponding phase will have a negative dc offset.

Figure 9 shows the current waveform with switching failure at

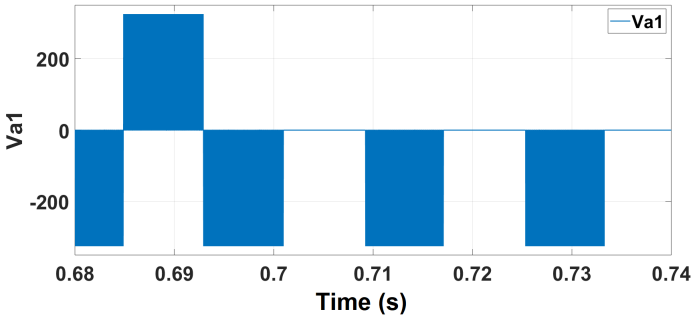

Fig. 8. Voltage Waveform with switching failure at t = 0.7 sec

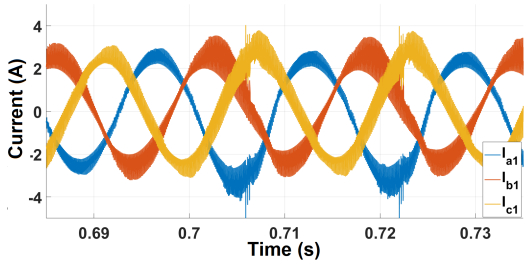

Fig. 9. Current Waveform with switching failure at t = 0.7 sec

t = 0.7 sec. It is observed from the current waveform that the current in phase I_{a1} has a negative dc offset after the fault. It can also be observed that the currents in the other two phases, i.e. I_{b1} and I_{c1} show a positive dc offset after occurrence of the fault. This positive offset is in response to balancing the effect of the negative offset in I_{a1}. *Figure* 10 and 11 show the speed and torque waveforms before and after the switching failure.

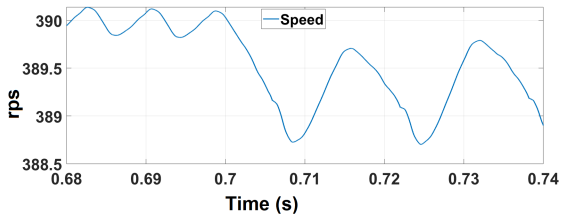

Fig. 10. Speed with switching failure at t = 0.7 sec

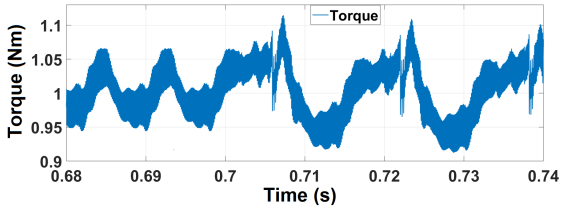

Fig. 11. Torque with switching failure at t = 0.7 sec

A decrease in the average speed and increase in the speed ripple is observed after the fault. Similarly, the torque ripple after the fault is $\approx 0.28Nm$ as compared to $\Delta T \approx 0.1Nm$ before fault.

Figure 12 represents the harmonic spectrum of the current

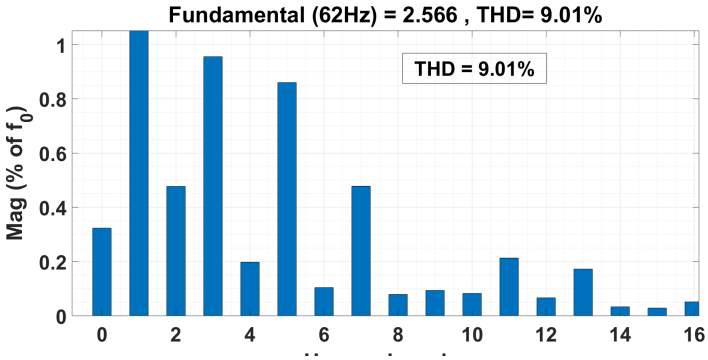

Fig. 12. Harmonic spectrum of I_{a1} under steady state condition

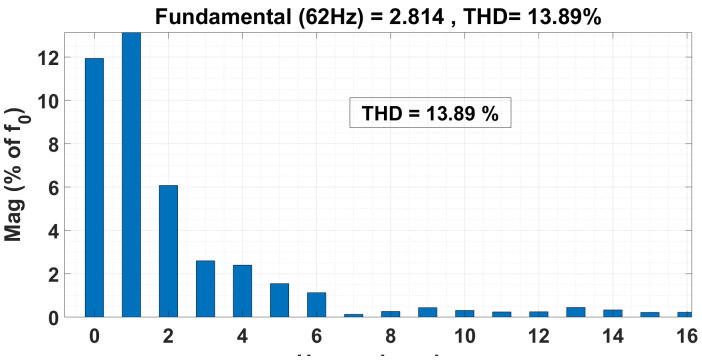

Fig. 13. Harmonic spectrum of I_{a1} after switching failure

I_{a1} before the fault and *Figure* 13 represents the harmonic spectrum after the fault has occurred. A higher THD (total

harmonic distortion) is observed in the post fault conditions. The harmonic spectrum under post fault conditions also shows a higher value of the dc component in the current. This higher dc harmonic can be taken as one of the fault signatures of a switching failure in one switch.

B. Open Phase Fault

Open phase fault represents a disconnection of one or more phases from the supply voltage. In this work this fault is simulated by disconnecting V_{a1} from the supply at t = 0.7 sec. *Figure* 14 shows the voltage waveform for this fault simulation. The machine is again assumed in steady state before the fault. *Figure* 15 is the current waveform before and after the fault. A general increase in the stator currents is observed.

Recalling that a stator current in one phase does not only

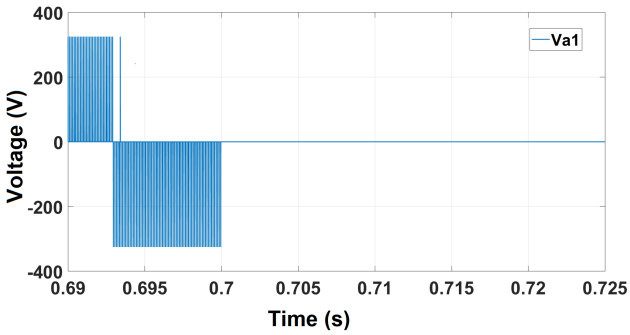

Fig. 14. Voltage waveform for open phase fault

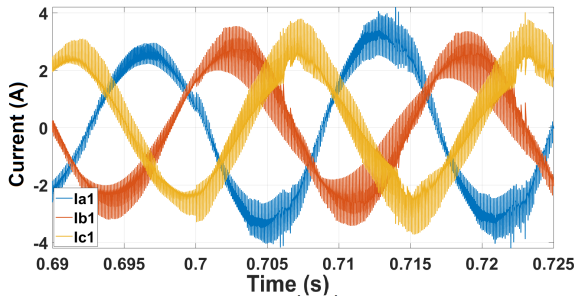

Fig. 15. Current waveform for open phase fault

depend on the voltage input to that phase but on all the voltage inputs. Due to inductive coupling (Equation (29) represents this relation in the frequency domain), current I_{a1} does not diminish to zero. Rather, due to strong couplings at the given synchronous frequency it is observed that the currents (*Figure* 15) increase in magnitude. This can be considered as a reaction to the reduced value of input to the system (*Figure* 14).

The speed of the PMSM experiences a decrease after the fault which is shown in *Figure* 16, though the speed ripple is approximately the same. The torque for this fault case, same as in the switching failure case (*Figure* 11), is observed to have a higher ripple of $\Delta T \approx 0.13Nm$.

Figure 18 shows the harmonic spectrum of the current in

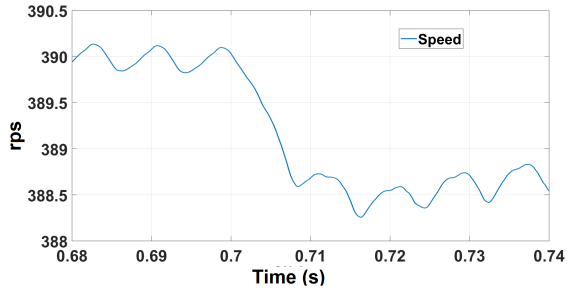

Fig. 16. Speed waveform for open phase fault at t = 0.7sec

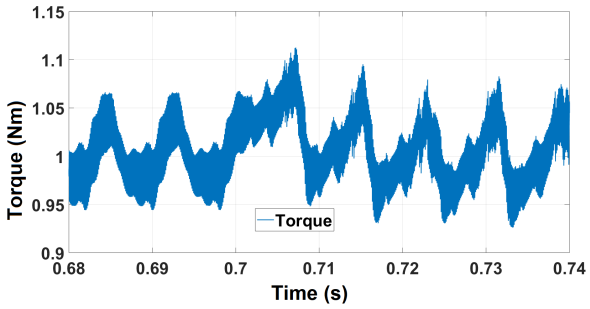

Fig. 17. Torque waveform for open phase fault at t = 0.7 sec

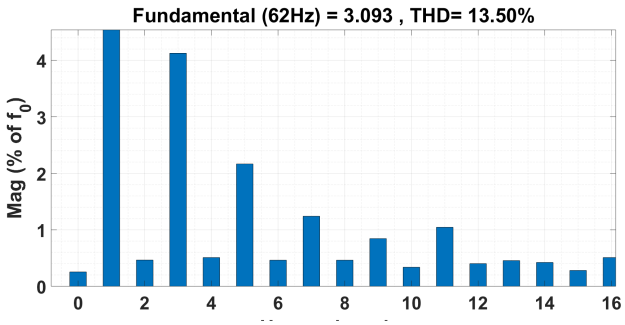

Fig. 18. Harmonic spectrum of I_{a1} after Open Phase Fault

phase *a1* after the fault. When compared with *Figure* 12 we observe an increase in the magnitude of all the odd harmonic components. This can be one of the fault signatures of an open phase fault but according to the author, might not serve the sole purpose of detecting an open phase fault. Also an increase in the THD is observed.

C. Phase-to-Phase Short Circuit Fault

One of the most common reasons for a short circuit fault in the phases is insulation failure which occurs due to friction between wires or mechanical wear due to long term use. In this work a short circuit fault is simulated by short circuiting phase *a1* and *b*1 at t = 0.7 sec. *Figure* 19 shows the voltage waveform for only V_{a1} for the fault before and after the fault occurrence. A short circuit fault is one of the most fatal faults to the machine as it can cause high currents in the machine, higher heating and eventually a machine shut down. Any kind of short circuit is immediately tackled with by isolating the

faulty phases and, or switches once the fault is detected. In this work we have assumed that none of the other failures in consequence to this short circuit occur, and proceed towards analyzing the effects of a phase-to-phase short circuit on the stator current, speed and torque. This also implies that the effects of heating of the machine are neglected, or the limits on current capacity of the switches, wire and other equipments are considered to be sufficiently high to be able to withstand this fault and allow a idealistic functioning of the machine.

Figure 20 shows the current waveform before and after the

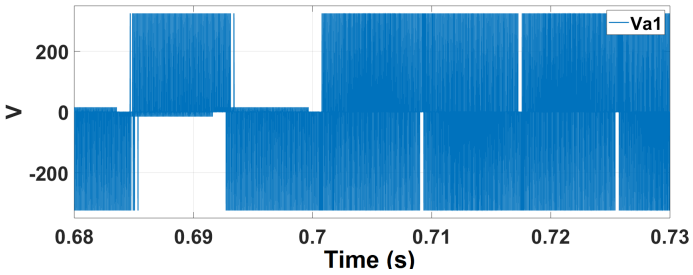

Fig. 19. Voltage waveform for phase-to-phase short circuit fault at t = 0.7 sec

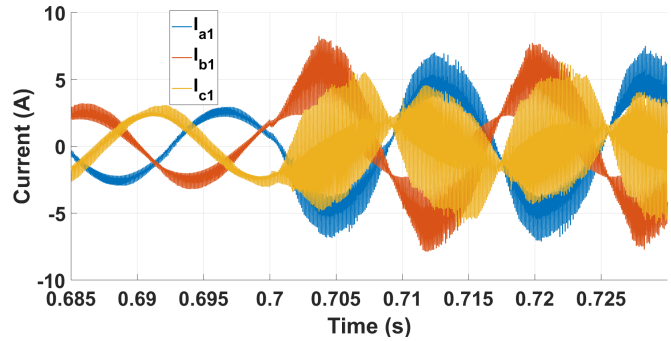

Fig. 20. Current waveform for phase-to-phase short circuit fault at t = 0.7 sec

fault occurrence. A high rise in the magnitude of all the currents is observed as expected due to a short circuit. Also a significantly higher distortion in the waveform from the sinusoidal wave is observed as compared to the previous fault cases (see *Figure* 9 and 15).

Figure 21 shows a high ripple in the speed after the fault.

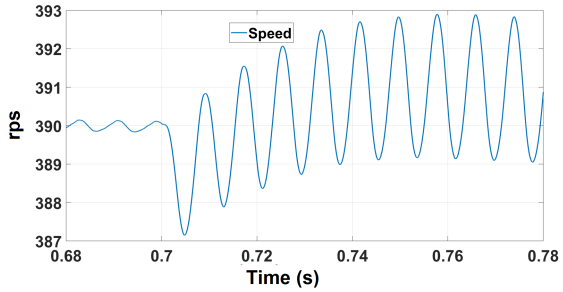

Fig. 21. Speed waveform for phase-to-phase short circuit fault at t = 0.7 sec

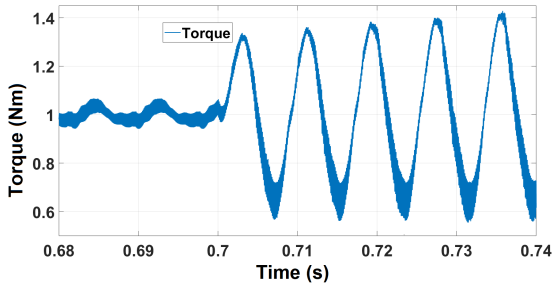

Fig. 22. Torque waveform for phase-to-phase short circuit fault at t = 0.7 sec

Similarly, *Figure* 22 shows a increase in the torque ripple ($\Delta T \approx 0.8Nm$ for $0.72sec < t < 0.73sec$) produced by the machine. This value of torque ripple is much higher when compared with the previous fault cases (see *Figure* 11 and 17).

Figure 23 shows the harmonic spectrum of the current

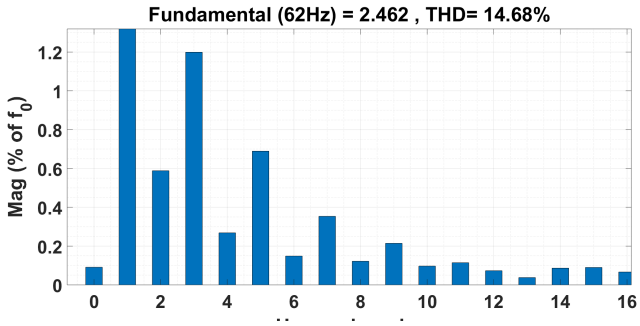

Fig. 23. Harmonic spectrum of I_{b1} at steady state conditions

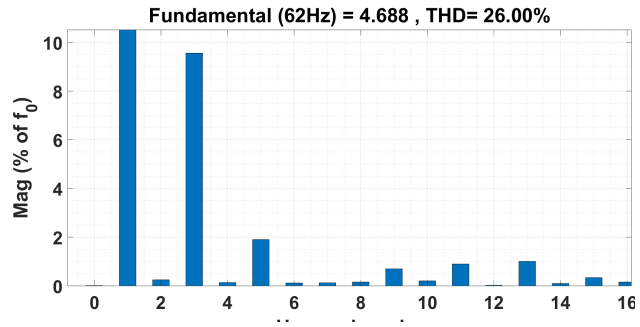

Fig. 24. Harmonic spectrum of I_{a1} under a phase-to-phase short circuit fault

in phase b1 under steady state conditions before the fault occurrence. The harmonic spectrum of current in phase *a1* is shown in *Figure* 12 and not reproduced in this section to avoid repetition. *Figure* 24 and 25 represent the harmonic spectrum of current in phase *a1* and *b1* under faulty conditions. The distinctive feature of a phase-to-phase short circuit fault, as observed from *Figure* 24 and 25, is increase in the third harmonic and very high THD post fault. The increase in the third harmonic can be expected due to the increase of unbalance in the circuit due to a phase-to-phase short circuit.

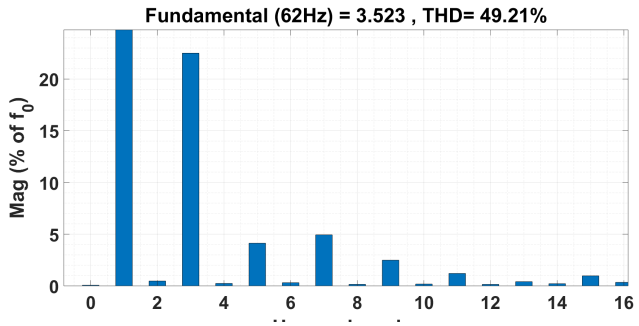

Fig. 25. Harmonic spectrum of I_{b1} under a phase-to-phase short circuit fault

V. Conclusion

Analytical model of 3×3 phase permanent magnet synchronous machine was successfully presented in this work. Sections IV-A, IV-B and IV-C provide a preliminary analysis of three kinds of faults in this machine. It can be concluded that an increase in the dc harmonic is the signature of a switching failure in one switch. Similarly increase in the odd harmonics and third harmonic in particular are the current signatures of open phase fault and phase-to-phase short circuit fault respectively. The simulations in this work are conducted on the analytical model of the PMSM. The model only considers a fundamental component of the magnetic field. A detailed model which takes into account and models higher frequency components in the 3×3 phase PMSM is required to deeply analyze the effects of these faults. The presence of a third harmonic in the current at steady state (*Figure* 12 and 23) could be due to the assumption $L_1 \approx L_2$ and a further analysis is required in this case as well.

Future Work

A model which incorporates the effects of all the significant harmonics in the 3×3 phase machine can be investigated. The simulation of faults needs to be studied taking into consideration necessary constraints on machine temperature, and current capacities. Also, fault modeling for different kinds of faults in a PMSM can be studied for a deeper insight. In this work the parameters of the machine are calculated based on assumptions in [2]. The parameter assumption needs to be validated using experimental data or mathematically. A finite element analysis can also be done in order to compare the results and a better understanding of the flux distribution.

References

[1] G. Renukadevi and K. Rajambal, "Modeling and analysis of multi-phase inverter fed induction motor drive with different phase numbers," *WSEAS Transactions on systems and Control*, vol. 8, no. 3, pp. 73–80, 2013.

[2] H. Kim, K. Shin, S. Englebretson, N. Frank, and W. Arshad, "Analytical model of multiphase permanent magnet synchronous machines for energy and transportation applications," in *2013 International Electric Machines & Drives Conference*, pp. 172–179, IEEE, 2013.

[3] B. Wang, G. Wei, J. Chu, and G. Yi, "A novel modeling for a dual three-phase permanent magnet synchronous machine," in *2008 10th International Conference on Control, Automation, Robotics and Vision*, pp. 1630–1634, IEEE, 2008.

[4] M. Kozovsky, P. Blaha, and P. Vaclavek, "Verification of nine-phase pmsm model in dq coordinates with mutual couplings," in *2016 6th IEEE International Conference on Control System, Computing and Engineering (ICCSCE)*, pp. 73–78, IEEE, 2016.

[5] E. Jung, H. Yoo, S.-K. Sul, H.-S. Choi, and Y.-Y. Choi, "A nine-phase permanent-magnet motor drive system for an ultrahigh-speed elevator," *IEEE Transactions on Industry Applications*, vol. 48, no. 3, pp. 987–995, 2012.

[6] T. Miller and M. McGilp, "Analysis of multi-phase permanent-magnet synchronous machines," in *2009 International Conference on Electrical Machines and Systems*, pp. 1–6, IEEE, 2009.

[7] A. S. Abdel-Khalik, A. M. Massoud, and S. Ahmed, "Nine-phase six-terminal induction machine modeling using vector space decomposition," *IEEE Transactions on Industrial Electronics*, vol. 66, no. 2, pp. 988–1000, 2019.

[8] J. Liu and W. Chen, "Generalized dq model of the permanent magnet synchronous motor based on extended park transformation," in *2013 1st International Future Energy Electronics Conference (IFEEC)*, pp. 885–890, IEEE, 2013.

[9] A. A. Rockhill and T. Lipo, "A simplified model of a nine-phase synchronous machine using vector space decomposition," *Electric Power Components and Systems*, vol. 38, no. 4, pp. 477–489, 2010.

[10] A. Djerdir, J. Farooq, A. Rezig, and A. Miraoui, "Faults in permanent magnet traction motors: State of the art and modelling approaches," in *IEEE PES General Meeting*, pp. 1–5, IEEE, 2010.

[11] O. V. Thorsen and M. Dalva, "Failure identification and analysis for high-voltage induction motors in the petrochemical industry," *IEEE Transactions on Industry Applications*, vol. 35, no. 4, pp. 810–818, 1999.

[12] D. Kastha and B. K. Bose, "Investigation of fault modes of voltage-fed inverter system for induction motor drive," *IEEE Transactions on Industry Applications*, vol. 30, no. 4, pp. 1028–1038, 1994.

[13] M. Fitouri, Y. BenSalem, and M. N. Abdelkrim, "Analysis and co-simulation of permanent magnet sychronous motor with short-circuit fault by finite element method," in *2016 13th International Multi-Conference on Systems, Signals & Devices (SSD)*, pp. 472–477, IEEE, 2016.

[14] M. Dai, A. Keyhani, and T. Sebastian, "Fault analysis of a pm brushless dc motor using finite element method," *IEEE Transactions on Energy Conversion*, vol. 20, no. 1, pp. 1–6, 2005.

[15] M. Wieczorek and E. Rosołowski, "Modelling of induction motor for simulation of internal faults," in *2010 Modern Electric Power Systems*, pp. 1–6, IEEE, 2010.

[16] M. Trabelsi, E. Semail, and N. K. Nguyen, "Experimental investigation of inverter open-circuit fault diagnosis for biharmonic five-phase permanent magnet drive," *IEEE Journal of Emerging and Selected Topics in Power Electronics*, vol. 6, no. 1, pp. 339–351, 2018.

[17] M. Salehifar, M. Moreno-Eguilaz, V. Sala, R. S. Arashloo, and L. Romeral, "Improved open switch fault detection based on normalized current analysis in multiphase fault tolerant converters," in *2013 9th IEEE International Symposium on Diagnostics for Electric Machines, Power Electronics and Drives (SDEMPED)*, pp. 512–519, IEEE, 2013.

[18] Y. L. Murphey, M. A. Masrur, Z. Chen, and B. Zhang, "Model-based fault diagnosis in electric drives using machine learning," *IEEE/ASME Transactions On Mechatronics*, vol. 11, no. 3, pp. 290–303, 2006.

[19] W. Le Roux, R. G. Harley, and T. G. Habetler, "Detecting rotor faults in low power permanent magnet synchronous machines," *IEEE Transactions on Power Electronics*, vol. 22, no. 1, pp. 322–328, 2007.

[20] A. Stavrou, H. G. Sedding, and J. Penman, "Current monitoring for detecting inter-turn short circuits in induction motors," *IEEE Transactions on energy conversion*, vol. 16, no. 1, pp. 32–37, 2001.

[21] J. O. Estima and A. J. M. Cardoso, "A new algorithm for real-time multiple open-circuit fault diagnosis in voltage-fed pwm motor drives by the reference current errors," *IEEE Transactions on Industrial Electronics*, vol. 60, no. 8, pp. 3496–3505, 2013.

[22] E. Yesilbag and L. Ergene, "Field oriented control of permanent magnet synchronous motors used in washers," in *2014 16th International Power Electronics and Motion Control Conference and Exposition*, pp. 1259–1264, IEEE, 2014.